

## Observation of new resonant structures in $\gamma\gamma \rightarrow \omega\phi$ , $\phi\phi$ and $\omega\omega$

Z. Q. Liu,<sup>13</sup> C. P. Shen,<sup>30</sup> C. Z. Yuan,<sup>13</sup> T. Iijima,<sup>31,30</sup> I. Adachi,<sup>9</sup> H. Aihara,<sup>53</sup> D. M. Asner,<sup>41</sup> V. Aulchenko,<sup>2</sup> T. Aushev,<sup>17</sup> A. M. Bakich,<sup>47</sup> K. Belous,<sup>15</sup> V. Bhardwaj,<sup>32</sup> B. Bhuyan,<sup>11</sup> M. Bischofberger,<sup>32</sup> A. Bondar,<sup>2</sup> A. Bozek,<sup>36</sup> M. Bračko,<sup>27,18</sup> T. E. Browder,<sup>8</sup> M.-C. Chang,<sup>4</sup> P. Chang,<sup>35</sup> A. Chen,<sup>33</sup> P. Chen,<sup>35</sup> B. G. Cheon,<sup>7</sup> R. Chistov,<sup>17</sup> I.-S. Cho,<sup>59</sup> K. Cho,<sup>21</sup> S.-K. Choi,<sup>6</sup> Y. Choi,<sup>46</sup> J. Dalseno,<sup>28,49</sup> Z. Doležal,<sup>3</sup> Z. Drásal,<sup>3</sup> S. Eidelman,<sup>2</sup> D. Epifanov,<sup>2</sup> J. E. Fast,<sup>41</sup> V. Gaur,<sup>48</sup> N. Gabyshev,<sup>2</sup> A. Garmash,<sup>2</sup> Y. M. Goh,<sup>7</sup> J. Haba,<sup>9</sup> K. Hayasaka,<sup>31</sup> H. Hayashii,<sup>32</sup> Y. Horii,<sup>31</sup> Y. Hoshi,<sup>51</sup> W.-S. Hou,<sup>35</sup> Y. B. Hsiung,<sup>35</sup> H. J. Hyun,<sup>23</sup> K. Inami,<sup>30</sup> A. Ishikawa,<sup>52</sup> R. Itoh,<sup>9</sup> M. Iwabuchi,<sup>59</sup> Y. Iwasaki,<sup>9</sup> T. Iwashita,<sup>32</sup> T. Julius,<sup>29</sup> J. H. Kang,<sup>59</sup> T. Kawasaki,<sup>38</sup> C. Kiesling,<sup>28</sup> H. J. Kim,<sup>23</sup> H. O. Kim,<sup>23</sup> J. B. Kim,<sup>22</sup> K. T. Kim,<sup>22</sup> M. J. Kim,<sup>23</sup> Y. J. Kim,<sup>21</sup> B. R. Ko,<sup>22</sup> S. Koblitz,<sup>28</sup> P. Kodyš,<sup>3</sup> S. Korpar,<sup>27,18</sup> P. Križan,<sup>25,18</sup> P. Krokovny,<sup>2</sup> T. Kumita,<sup>55</sup> A. Kuzmin,<sup>2</sup> Y.-J. Kwon,<sup>59</sup> J. S. Lange,<sup>5</sup> S.-H. Lee,<sup>22</sup> J. Li,<sup>45</sup> X. R. Li,<sup>45</sup> Y. Li,<sup>57</sup> J. Libby,<sup>12</sup> C. Liu,<sup>44</sup> D. Liventsev,<sup>17</sup> R. Louvot,<sup>24</sup> D. Matvienko,<sup>2</sup> S. McOnie,<sup>47</sup> K. Miyabayashi,<sup>32</sup> H. Miyata,<sup>38</sup> Y. Miyazaki,<sup>30</sup> R. Mizuk,<sup>17</sup> G. B. Mohanty,<sup>48</sup> A. Moll,<sup>28,49</sup> T. Mori,<sup>30</sup> N. Muramatsu,<sup>42</sup> R. Mussa,<sup>16</sup> Y. Nagasaka,<sup>10</sup> E. Nakano,<sup>40</sup> M. Nakao,<sup>9</sup> H. Nakazawa,<sup>33</sup> C. Ng,<sup>53</sup> S. Nishida,<sup>9</sup> K. Nishimura,<sup>8</sup> O. Nitoh,<sup>56</sup> T. Nozaki,<sup>9</sup> S. Ogawa,<sup>50</sup> T. Ohshima,<sup>30</sup> S. Okuno,<sup>19</sup> S. L. Olsen,<sup>45,8</sup> Y. Onuki,<sup>53</sup> P. Pakhlov,<sup>17</sup> G. Pakhlova,<sup>17</sup> C. W. Park,<sup>46</sup> H. K. Park,<sup>23</sup> T. K. Pedlar,<sup>26</sup> R. Pestotnik,<sup>18</sup> M. Petrič,<sup>18</sup> L. E. Piilonen,<sup>57</sup> M. Ritter,<sup>28</sup> M. Röhrken,<sup>20</sup> S. Ryu,<sup>45</sup> H. Sahoo,<sup>8</sup> K. Sakai,<sup>9</sup> Y. Sakai,<sup>9</sup> T. Sanuki,<sup>52</sup> Y. Sato,<sup>52</sup> O. Schneider,<sup>24</sup> C. Schwanda,<sup>14</sup> R. Seidl,<sup>43</sup> K. Senyo,<sup>58</sup> M. E. Sevier,<sup>29</sup> M. Shapkin,<sup>15</sup> V. Shebalin,<sup>2</sup> T.-A. Shibata,<sup>54</sup> J.-G. Shiu,<sup>35</sup> B. Shwartz,<sup>2</sup> A. Sibidanov,<sup>47</sup> F. Simon,<sup>28,49</sup> P. Smerkol,<sup>18</sup> Y.-S. Sohn,<sup>59</sup> A. Sokolov,<sup>15</sup> E. Solovieva,<sup>17</sup> S. Stanič,<sup>39</sup> M. Starič,<sup>18</sup> T. Sumiyoshi,<sup>55</sup> G. Tatishvili,<sup>41</sup> Y. Teramoto,<sup>40</sup> M. Uchida,<sup>54</sup> S. Uehara,<sup>9</sup> T. Uglov,<sup>17</sup> Y. Unno,<sup>7</sup> S. Uno,<sup>9</sup> P. Urquijo,<sup>1</sup> G. Varner,<sup>8</sup> A. Vinokurova,<sup>2</sup> V. Vorobyev,<sup>2</sup> C. H. Wang,<sup>34</sup> P. Wang,<sup>13</sup> X. L. Wang,<sup>13</sup> M. Watanabe,<sup>38</sup> Y. Watanabe,<sup>19</sup> K. M. Williams,<sup>57</sup> E. Won,<sup>22</sup> Y. Yamashita,<sup>37</sup> Y. Yusa,<sup>38</sup> C. C. Zhang,<sup>13</sup> Z. P. Zhang,<sup>44</sup> V. Zhilich,<sup>2</sup> and V. Zhulanov<sup>2</sup>

(The Belle Collaboration)

<sup>1</sup>University of Bonn, Bonn

<sup>2</sup>Budker Institute of Nuclear Physics SB RAS and Novosibirsk State University, Novosibirsk 630090

<sup>3</sup>Faculty of Mathematics and Physics, Charles University, Prague

<sup>4</sup>Department of Physics, Fu Jen Catholic University, Taipei

<sup>5</sup>Justus-Liebig-Universität Gießen, Gießen

<sup>6</sup>Gyeongsang National University, Chinju

<sup>7</sup>Hanyang University, Seoul

<sup>8</sup>University of Hawaii, Honolulu, Hawaii 96822

<sup>9</sup>High Energy Accelerator Research Organization (KEK), Tsukuba

<sup>10</sup>Hiroshima Institute of Technology, Hiroshima

<sup>11</sup>Indian Institute of Technology Guwahati, Guwahati

<sup>12</sup>Indian Institute of Technology Madras, Madras

<sup>13</sup>Institute of High Energy Physics, Chinese Academy of Sciences, Beijing

<sup>14</sup>Institute of High Energy Physics, Vienna

<sup>15</sup>Institute of High Energy Physics, Protvino

<sup>16</sup>INFN - Sezione di Torino, Torino

<sup>17</sup>Institute for Theoretical and Experimental Physics, Moscow

<sup>18</sup>J. Stefan Institute, Ljubljana

<sup>19</sup>Kanagawa University, Yokohama

<sup>20</sup>Institut für Experimentelle Kernphysik, Karlsruher Institut für Technologie, Karlsruhe

<sup>21</sup>Korea Institute of Science and Technology Information, Daejeon

<sup>22</sup>Korea University, Seoul

<sup>23</sup>Kyungpook National University, Taegu

<sup>24</sup>École Polytechnique Fédérale de Lausanne (EPFL), Lausanne

<sup>25</sup>Faculty of Mathematics and Physics, University of Ljubljana, Ljubljana

- <sup>26</sup>Luther College, Decorah, Iowa 52101  
<sup>27</sup>University of Maribor, Maribor  
<sup>28</sup>Max-Planck-Institut für Physik, München  
<sup>29</sup>University of Melbourne, School of Physics, Victoria 3010  
<sup>30</sup>Graduate School of Science, Nagoya University, Nagoya  
<sup>31</sup>Kobayashi-Maskawa Institute, Nagoya University, Nagoya  
<sup>32</sup>Nara Women's University, Nara  
<sup>33</sup>National Central University, Chung-li  
<sup>34</sup>National United University, Miao Li  
<sup>35</sup>Department of Physics, National Taiwan University, Taipei  
<sup>36</sup>H. Niewodniczanski Institute of Nuclear Physics, Krakow  
<sup>37</sup>Nippon Dental University, Niigata  
<sup>38</sup>Niigata University, Niigata  
<sup>39</sup>University of Nova Gorica, Nova Gorica  
<sup>40</sup>Osaka City University, Osaka  
<sup>41</sup>Pacific Northwest National Laboratory, Richland, Washington 99352  
<sup>42</sup>Research Center for Nuclear Physics, Osaka University, Osaka  
<sup>43</sup>RIKEN BNL Research Center, Upton, New York 11973  
<sup>44</sup>University of Science and Technology of China, Hefei  
<sup>45</sup>Seoul National University, Seoul  
<sup>46</sup>Sungkyunkwan University, Suwon  
<sup>47</sup>School of Physics, University of Sydney, NSW 2006  
<sup>48</sup>Tata Institute of Fundamental Research, Mumbai  
<sup>49</sup>Excellence Cluster Universe, Technische Universität München, Garching  
<sup>50</sup>Toho University, Funabashi  
<sup>51</sup>Tohoku Gakuin University, Tagajo  
<sup>52</sup>Tohoku University, Sendai  
<sup>53</sup>Department of Physics, University of Tokyo, Tokyo  
<sup>54</sup>Tokyo Institute of Technology, Tokyo  
<sup>55</sup>Tokyo Metropolitan University, Tokyo  
<sup>56</sup>Tokyo University of Agriculture and Technology, Tokyo  
<sup>57</sup>CNP, Virginia Polytechnic Institute and State University, Blacksburg, Virginia 24061  
<sup>58</sup>Yamagata University, Yamagata  
<sup>59</sup>Yonsei University, Seoul

The processes  $\gamma\gamma \rightarrow \omega\phi$ ,  $\phi\phi$ , and  $\omega\omega$  are measured using an  $870 \text{ fb}^{-1}$  data sample collected with the Belle detector at the KEKB asymmetric-energy  $e^+e^-$  collider. Production of vector meson pairs is clearly observed and their cross sections are measured for masses that range from threshold to 4.0 GeV. In addition to signals from well established spin-zero and spin-two charmonium states, there are resonant structures below charmonium threshold, which have not been previously observed. We report a spin-parity analysis for the new structures and determine the products of the  $\eta_c$ ,  $\chi_{c0}$ , and  $\chi_{c2}$  two-photon decay widths and branching fractions to  $\omega\phi$ ,  $\phi\phi$ , and  $\omega\omega$ .

PACS numbers: 14.40.-n, 13.25.Gv, 13.25.Jx, 13.66.Bc

A plethora of states, especially many new charmonium or charmonium-like states (the so called “XYZ particles”), that are not easily accommodated within the quark model picture of hadrons have been observed [1]. Recently a clear signal for a new state  $X(3915) \rightarrow \omega J/\psi$  [2] and evidence for another state  $X(4350) \rightarrow \phi J/\psi$  [3] have been reported, thereby introducing new puzzles to charmonium or charmonium-like spectroscopy.

Since these states couple to a  $J/\psi$  and a light mass vector, some authors have suggested that they are good candidates for molecular or tetraquark states [1].

It is natural to extend the above theoretical picture to similar states coupling to  $\omega\phi$ , since the only difference between such states and the  $X(3915)$  [2] or  $X(4350)$  [3] is the replacement of the  $c\bar{c}$  pair with a pair of light quarks.

States coupling to  $\omega\omega$  or  $\phi\phi$ , although not as exotic as those that decay into  $\omega\phi$ , which have two pairs of light quarks in different generations, could also provide information on the classification of the low-lying states coupled to pairs of light vector mesons.

Experimental studies of  $\gamma\gamma \rightarrow VV$  ( $V = \rho, \omega, \phi, K^*$ ) began in 1980 with the measurement of  $\gamma\gamma \rightarrow \rho^0\rho^0$  [4], and later  $\gamma\gamma \rightarrow \rho^+\rho^-$  [5]. A number of theoretical models, such as  $q^2\bar{q}^2$  tetraquark states [6], Regge exchange [7], and an  $s$ -channel  $\rho^0\rho^0$  resonance [8], were proposed to explain the large cross section observed in  $\gamma\gamma \rightarrow \rho^0\rho^0$  near the  $\rho^0\rho^0$  threshold that is absent in  $\gamma\gamma \rightarrow \rho^+\rho^-$  [9]. The  $\gamma\gamma \rightarrow \omega\phi$  and  $\omega\omega$  processes were studied by the ARGUS Collaboration [10, 11] with very limited statistics, while  $\gamma\gamma \rightarrow \phi\phi$  has never been measured below the charmonium mass region.

In this Letter, we report measurements of the cross sections for  $\gamma\gamma \rightarrow VV$ , where  $VV = \omega\phi, \phi\phi$  and  $\omega\omega$ , as well as observations of new resonant structures below charmonium threshold. The results are based on an analysis of an  $870 \text{ fb}^{-1}$  data sample taken at or near the  $\Upsilon(nS)$  ( $n = 1, \dots, 5$ ) resonances with the Belle detector [12] operating at the KEKB asymmetric-energy  $e^+e^-$  collider [13]. The Belle detector is described in detail elsewhere [12]. We use the program TREPS [14] to generate signal Monte Carlo (MC) events and determine experimental efficiencies and luminosities.

We require four reconstructed charged tracks with zero net charge. The selections of the charged kaon and pion tracks are the same as in Ref. [15]. With this selection, the kaon (pion) identification efficiency is about 97% (98%), while 0.4% (1.0%) of kaons (pions) are misidentified as pions (kaons). A similar likelihood ratio is formed for electron identification [16]. Photon conversion backgrounds are removed if any charged track in an event is identified as electron or positron ( $\mathcal{R}_e > 0.9$ ). For  $\gamma\gamma \rightarrow \phi\phi$ , we require that only three of the charged tracks be identified as kaons.

A good neutral cluster is reconstructed as a photon if its electromagnetic calorimeter (ECL) shower does not match the extrapolation of any charged track and its energy is greater than 50 MeV. The  $\pi^0$  candidates are reconstructed from pairs of photons with invariant mass within  $15 \text{ MeV}/c^2$  of the  $\pi^0$  nominal mass. Here the  $\pi^0$  mass resolution is about  $6 \text{ MeV}/c^2$  from MC simulation. A mass-constrained kinematic fit is applied to the selected  $\pi^0$  candidate and  $\chi^2 < 10$  is required. For  $\gamma\gamma \rightarrow \omega\omega$ , the energies of the photons from  $\pi^0$  decays are further required to be greater than 75 MeV in the endcap ECL region ( $\cos\theta_\gamma < -0.65$ ) to suppress background with misreconstructed photons. When there are more than two  $\pi^0$  candidates in an event, the pair with the smallest  $\chi^2$  sum from the mass constraint is retained. To suppress backgrounds with extra neutral clusters in the  $\omega\phi$  and  $\omega\omega$  modes, events are removed if there are

additional photons with energy greater than 160 MeV.

We define the  $\omega$  signal region as  $0.762 \text{ GeV}/c^2 < M(\pi^+\pi^-\pi^0) < 0.802 \text{ GeV}/c^2$ , and the  $\omega$  mass sidebands region as  $0.702 \text{ GeV}/c^2 < M(\pi^+\pi^-\pi^0) < 0.742 \text{ GeV}/c^2$  or  $0.822 \text{ GeV}/c^2 < M(\pi^+\pi^-\pi^0) < 0.862 \text{ GeV}/c^2$ , which is twice as wide as the signal region. The  $\phi$  signal region is defined as  $1.012 \text{ GeV}/c^2 < M(K^+K^-) < 1.027 \text{ GeV}/c^2$ , and its sideband regions are defined as  $0.99 \text{ GeV}/c^2 < M(K^+K^-) < 1.005 \text{ GeV}/c^2$  or  $1.034 \text{ GeV}/c^2 < M(K^+K^-) < 1.049 \text{ GeV}/c^2$ . The  $\phi$  sidebands are also twice as wide as the signal region. The  $VV$  pair sideband is defined as one  $V$  in the signal region while the other in the  $V$  mass sideband. For the two possible combinations of  $\phi\phi$  in the  $2(K^+K^-)$  final state, the one with the smallest  $\delta_{min} = \sqrt{(M(K^+K^-)_1 - m_\phi)^2 + (M(K^+K^-)_2 - m_\phi)^2}$  is chosen. For the four possible combinations of  $\omega\omega$ , only one combination from a true signal can survive after event selection.

The magnitude of the vector sum of the final particles' transverse momenta in the  $e^+e^-$  center-of-mass (C.M.) frame,  $|\sum \vec{P}_t^*|$ , which approximates the transverse momentum of the two-photon-collision system, is used as a discriminating variable to separate signal from background. The signal tends to accumulate at small  $|\sum \vec{P}_t^*|$  values while the non- $\gamma\gamma$  background is distributed over a wider range. We obtain the number of  $VV$  events in each  $VV$  invariant mass bin by fitting the  $|\sum \vec{P}_t^*|$  distribution between zero and  $0.9 \text{ GeV}/c$ . The signal shape is from MC simulation of the signal mode and the background shape is parameterized as a second-order Chebyshev polynomial. In order to control the background shape, we restrict the coefficients of the background polynomials in nearby invariant mass bins to vary smoothly. The resulting  $VV$  invariant mass distributions are shown in Fig. 1.

There are some obvious structures in the low  $VV$  invariant mass region in Fig. 1. Two-dimensional (2D) angular distributions are investigated to obtain the  $J^P$  of the structures. In the process  $\gamma\gamma \rightarrow VV$ , five angles are kinematically independent. Among the possible variable sets, we choose  $z, z^*, z^{**}, \phi^*$ , and  $\phi^{**}$  [17] and use the transversity angle ( $\phi_T$ ) and polar-angle product ( $\Pi_\theta$ ) variables to analyze the angular distributions. They are defined as  $\phi_T = |\phi^* + \phi^{**}|/2\pi$ ,  $\Pi_\theta = [1 - (z^*)^2][1 - (z^{**})^2]$ .

We obtain the number of signal events by fitting the  $|\sum \vec{P}_t^*|$  distribution in each  $\phi_T$  and  $\Pi_\theta$  bin in the 2D space, which is divided into  $4 \times 4, 5 \times 5$ , and  $10 \times 10$  bins for  $\omega\phi, \phi\phi$ , and  $\omega\omega$ , respectively, for  $M(VV) < 2.8 \text{ GeV}/c^2$ , in some wider  $VV$  mass bins as shown in Fig. 2. The obtained 2D angular distribution data are fitted with the signal shapes from MC-simulated samples with different  $J^P$  assumptions ( $0^+, 0^-, 2^+, 2^-$ ). We find: (1) for  $\omega\phi$ :  $0^+$  ( $S$ -wave) or  $2^+$  ( $S$ -wave) can describe data with  $\chi^2/ndf = 1.1$  or  $1.2$ , while a mixture of  $0^+$  ( $S$ -

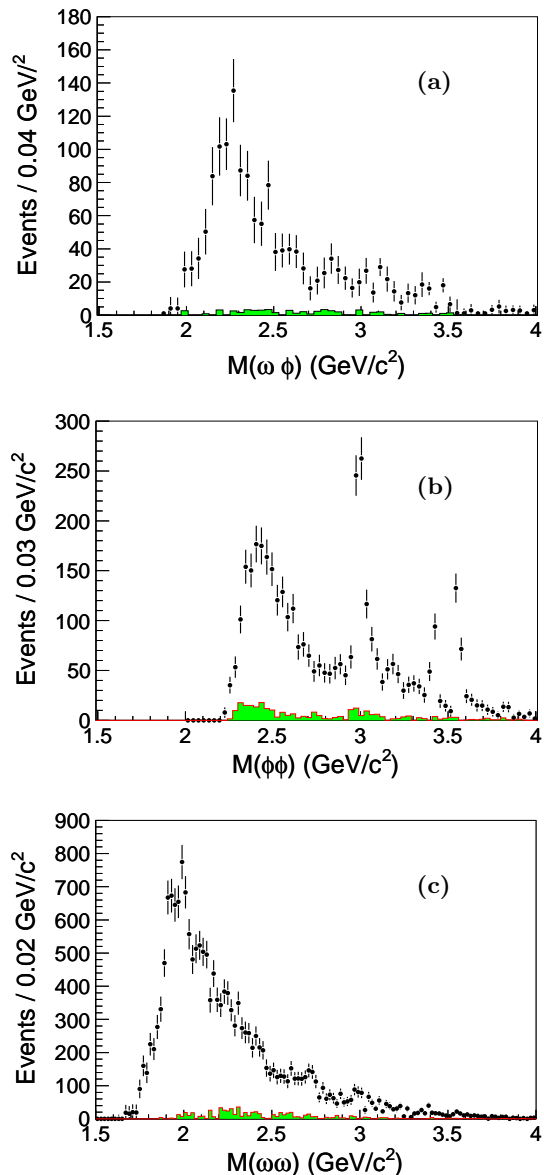


FIG. 1: The (a)  $\omega\phi$ , (b)  $\phi\phi$  and (c)  $\omega\omega$  invariant mass distributions obtained by fitting the  $|\sum \vec{P}_t^*|$  distribution in each  $VV$  mass bin. The shaded histograms are from the corresponding normalized sidebands, which will be subtracted in calculating the final cross sections.

wave) and  $2^+$  ( $S$ -wave) describes data with  $\chi^2/ndf = 0.9$  ( $ndf$  is the number of degrees of freedom); (2) for  $\phi\phi$ : a mixture of  $0^+$  ( $S$ -wave) and  $2^-$  ( $P$ -wave) describes data with  $\chi^2/ndf = 1.3$ ; and (3) for  $\omega\omega$ : a mixture of  $0^+$  ( $S$ -wave) and  $2^+$  ( $S$ -wave) describes data with  $\chi^2/ndf = 1.3$ . The contributions from other  $J^P$  are found to be small and thus neglected.

The cross section  $\sigma_{\gamma\gamma \rightarrow VV}(W_{\gamma\gamma})$  is calculated from

$$\sigma_{\gamma\gamma \rightarrow VV}(W_{\gamma\gamma}) = \frac{\Delta n}{\frac{dL_{\gamma\gamma}}{dW_{\gamma\gamma}} \epsilon(W_{\gamma\gamma}) \Delta W_{\gamma\gamma}}, \quad (1)$$

where  $\frac{dL_{\gamma\gamma}}{dW_{\gamma\gamma}}$  is the differential luminosity of the two-photon collision, and  $\epsilon$  is the efficiency. Here  $\Delta W_{\gamma\gamma}$  is the bin width and  $\Delta n$  is the number of events in the  $\Delta W_{\gamma\gamma}$  bin.

The  $\gamma\gamma \rightarrow VV$  cross sections are shown in Fig. 2. For the processes  $\gamma\gamma \rightarrow \omega\phi$  and  $\phi\phi$ , the cross sections are measured in the C.M. angular range  $|\cos\theta^*| < 0.8$  since there are no detected events beyond this limit, while for  $\omega\omega$  the full  $\cos\theta^*$  range is covered. The cross sections for different  $J^P$  values as a function of  $M(VV)$  are also shown in Fig. 2. We observe structures at  $M(\omega\phi) \sim 2.2 \text{ GeV}/c^2$ ,  $M(\phi\phi) \sim 2.35 \text{ GeV}/c^2$ , and  $M(\omega\omega) \sim 1.91 \text{ GeV}/c^2$  with peak cross sections of  $(0.27 \pm 0.05) \text{ nb}$ ,  $(0.30 \pm 0.04) \text{ nb}$ , and  $(5.30 \pm 0.42) \text{ nb}$ , respectively. While there are substantial spin-zero components in all three modes, there are also significant spin-two components, at least in the  $\phi\phi$  and  $\omega\omega$  modes. The phase space enhancement effect should be much closer to the  $VV$  mass thresholds and it is impossible to produce the observed mass-dependent cross sections.

The inset also shows the distribution of the cross section on a semi-logarithmic scale, where, in the high mass region, we fit the  $W_{\gamma\gamma}^{-n}$  dependence of the cross section. The solid curves are the fitted results; the fit gives  $n = 7.2 \pm 0.6$ ,  $8.4 \pm 1.1$ , and  $9.1 \pm 0.6$  for the  $\omega\phi$ ,  $\omega\omega$ , and  $\phi\phi$  modes, respectively. These results are consistent with the predictions from pQCD and handbag models [18], and similar to previous measurements in other modes [19].

There are several sources of systematic error for the cross section measurements. The particle identification uncertainties are 1.5% for each kaon, 1.2% for each pion. A momentum-weighted systematic error in tracking efficiency is taken for each track, which is about 0.6%. The efficiency uncertainties associated with the  $\omega$  and  $\phi$  mass requirements are almost independent of the  $VV$  mass, and are estimated to be 1.9% and 1.6%, respectively. The statistical error in the MC samples is about 0.5%. The accuracy of the two-photon luminosity function calculated with the TREPS generator is estimated to be about 5% including the error from neglecting radiative corrections (2%), the uncertainty from the form factor effect (2%), and the uncertainty in the total integrated luminosity (1.4%) [14]. The uncertainty of the trigger simulation is smaller than 5% [20]. The preselection efficiency for the final states has little dependence on the  $VV$  invariant mass, with an uncertainty that is smaller than 1% for  $\omega\phi$ , 4% for  $\phi\phi$  and 2.5% for  $\omega\omega$ . From Ref. [21], the uncertainty in the world average values for  $\mathcal{B}(\phi \rightarrow K^+K^-)$  is 1.1% and that for  $\mathcal{B}(\omega \rightarrow \pi^+\pi^-\pi^0)$  is 0.8%. The uncertainty in the fitted yield for the signal is estimated by varying the order of the background polynomial and fit range, which is 10% for  $\omega\phi$ , 2.5% for  $\phi\phi$ , and 4.0% for  $\omega\omega$ . The uncertainty on the  $|\sum \vec{P}_t^*|$  resolution is smaller than 2.2%, which is estimated by changing the MC signal

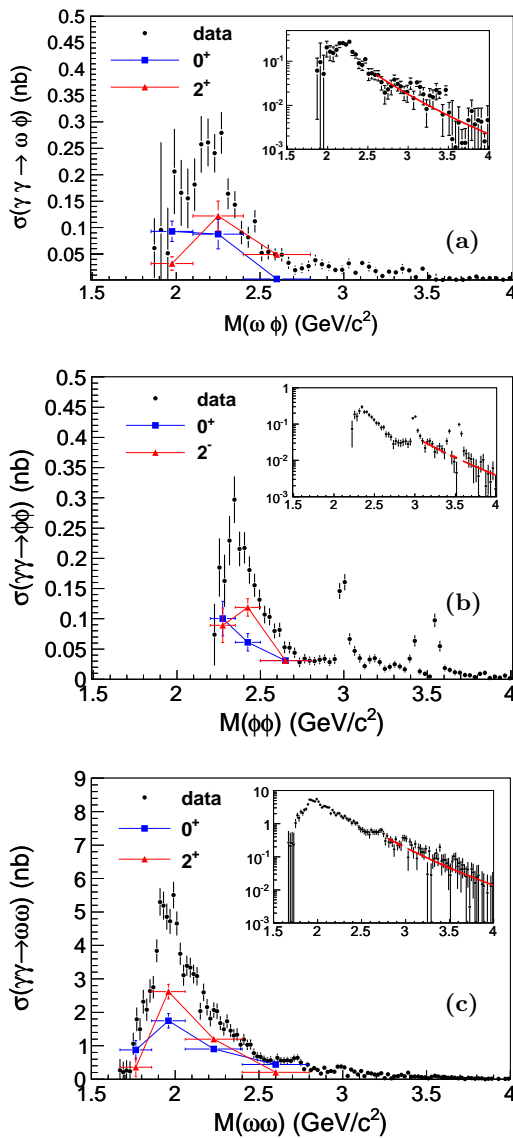


FIG. 2: The cross sections of  $\gamma\gamma \rightarrow \omega\phi$  (a),  $\phi\phi$  (b), and  $\omega\omega$  (c) are shown as points with error bars. The cross sections for different  $J^P$  values as a function of  $M(VV)$  are shown as the triangles and squares with error bars. For the processes  $\gamma\gamma \rightarrow \omega\phi$  and  $\phi\phi$ , the cross sections are measured in the C.M. angular range  $|\cos\theta^*| < 0.8$ , while for  $\omega\omega$  the full  $\cos\theta^*$  range is covered. The error bars are statistical only; there are overall systematic errors of 15%, 11% and 13% for  $\omega\phi$ ,  $\phi\phi$  and  $\omega\omega$ , respectively. The inset also shows the cross section on a semi-logarithmic scale. In the high energy region, the solid curve shows a fit to a  $W_{\gamma\gamma}^{-n}$  dependence for the cross section after the significant charmonium contributions ( $\eta_c$ ,  $\chi_{c0}$  and  $\chi_{c2}$ ) were excluded.

resolution by  $\pm 10\%$ . The uncertainty on the weighted efficiency curve is estimated by changing the fitted ratio of the  $J^P$  components by  $\pm 1\sigma$ , which is 1.0% for  $\omega\phi$ , 3.1% for  $\phi\phi$ , and 1.0% for  $\omega\omega$ . Assuming that all of these systematic error sources are independent, we add them in

quadrature to obtain the total systematic errors, which are 15%, 11% and 13% for  $\omega\phi$ ,  $\phi\phi$  and  $\omega\omega$ , respectively.

For  $VV$  invariant masses above 2.8  $\text{GeV}/c^2$ , we measure the production rate of charmonium states. In measuring the production rates,  $|\sum \bar{P}_t^*|$  is required to be less than 0.1  $\text{GeV}/c$  in order to reduce backgrounds from non-two-photon-processes and two-photon-processes with extra particles other than  $\phi$  or  $\omega$  in the final state.

Figure 3 shows the  $VV$  invariant mass distributions and best fits. Clear  $\eta_c$ ,  $\chi_{c0}$  and  $\chi_{c2} \rightarrow \phi\phi$ , and  $\eta_c \rightarrow \omega\omega$  signals are evident. The  $VV$  mass distributions are fitted with three incoherent Breit-Wigner functions convoluted with a corresponding double Gaussian resolution function as the  $\eta_c$ ,  $\chi_{c0}$  and  $\chi_{c2}$  signal shapes, and a second-order Chebyshev polynomial as the background shape.

The numbers of signal events and product of the two-photon decay width and branching fraction  $\Gamma_{\gamma\gamma}\mathcal{B}(X \rightarrow VV)$  (or the upper limits in case the signal is insignificant) for  $\eta_c$ ,  $\chi_{c0}$  and  $\chi_{c2}$  are listed in Table I. In these calculations, we assume there is no interference between the charmonium and the continuum amplitudes [22]. A systematic error estimate similar to that for the cross sections considers additionally the uncertainties on the resonance parameters and results in the total systematic errors of 13%, 11%, and 11% for  $\Gamma_{\gamma\gamma}(R)\mathcal{B}(R \rightarrow \omega\phi)$ ; 7.9%, 8.0%, and 7.2% for  $\Gamma_{\gamma\gamma}(R)\mathcal{B}(R \rightarrow \phi\phi)$ ; and 11%, 10%, and 9.1% for  $\Gamma_{\gamma\gamma}(R)\mathcal{B}(R \rightarrow \omega\omega)$ , for  $R = \eta_c$ ,  $\chi_{c0}$  and  $\chi_{c2}$ , respectively. For the upper limit determinations, the efficiencies have been lowered by a factor of  $1 - \sigma_{\text{sys}}$  in order to obtain conservative values. The measurements of  $\Gamma_{\gamma\gamma}\mathcal{B}(X \rightarrow \phi\phi)$  for  $\eta_c$ ,  $\chi_{c0}$  and  $\chi_{c2}$  are consistent with previously published results [20] with improved precision. The values of  $\Gamma_{\gamma\gamma}\mathcal{B}(X \rightarrow \phi\phi)$  for  $\eta_c$ ,  $\chi_{c0}$  and  $\chi_{c2}$  obtained in this work supersede those in Ref. [20]. All the other results are first measurements.

In summary, we present a search for exotic states in two-photon processes  $\gamma\gamma \rightarrow \omega\phi$ ,  $\phi\phi$  and  $\omega\omega$ . The production of  $\omega\phi$ ,  $\phi\phi$ , and  $\omega\omega$  is observed, and cross sections are measured up to 4  $\text{GeV}/c^2$ . The cross sections for  $\gamma\gamma \rightarrow \omega\phi$  are much lower than the prediction of the  $q^2\bar{q}^2$  tetraquark model [9] of 1 nb, while the resonant structure in the  $\gamma\gamma \rightarrow \phi\phi$  mode is nearly at the predicted position. However, the  $\phi\phi$  cross section is an order of magnitude lower than the expectation in the tetraquark model. On the other hand, the t-channel factorization model [23] predicted that the  $\phi\phi$  cross sections vary between 0.001 nb and 0.05 nb in the mass region of 2.0  $\text{GeV}/c^2$  to 5.0  $\text{GeV}/c^2$ , which are much lower than the experimental data. For  $\gamma\gamma \rightarrow \omega\omega$ , the t-channel factorization model [23] predicted a broad structure between 1.8  $\text{GeV}/c^2$  and 3.0  $\text{GeV}/c^2$  with a peak cross section of 10-30 nb near 2.2  $\text{GeV}/c^2$ , while the one-pion-exchange model [24] predicted an enhancement near threshold around 1.6  $\text{GeV}/c^2$  with a peak cross section of 13 nb using a preferred value of the slope parameter.

TABLE I: Results for  $\Gamma_{\gamma\gamma}\mathcal{B}(X \rightarrow VV)$  (eV) and the numbers of events (in brackets) for  $\eta_c$ ,  $\chi_{c0}$  and  $\chi_{c2}$ , where the values of  $\mathcal{B}(\omega \rightarrow \pi^+\pi^-\pi^0) = (89.2 \pm 0.7)\%$  and  $\mathcal{B}(\phi \rightarrow K^+K^-) = (48.9 \pm 0.5)\%$  are used [21]. The first and second errors for the central values are statistical and systematic, respectively. The upper limits are obtained at the 90% confidence level with systematic errors included.

Mode	$\omega\phi$	$\phi\phi$	$\omega\omega$
$\eta_c$	$< 0.49$ [ $< 7.9$ ]	$7.75 \pm 0.66 \pm 0.62$ [ $386 \pm 31$ ]	$8.67 \pm 2.86 \pm 0.96$ [ $85 \pm 29$ ]
$\chi_{c0}$	$< 0.34$ [ $< 4.3$ ]	$1.72 \pm 0.33 \pm 0.14$ [ $56 \pm 11$ ]	$< 3.9$ [ $< 35$ ]
$\chi_{c2}$	$< 0.04$ [ $< 2.4$ ]	$0.62 \pm 0.07 \pm 0.05$ [ $89 \pm 11$ ]	$< 0.64$ [ $< 28$ ]

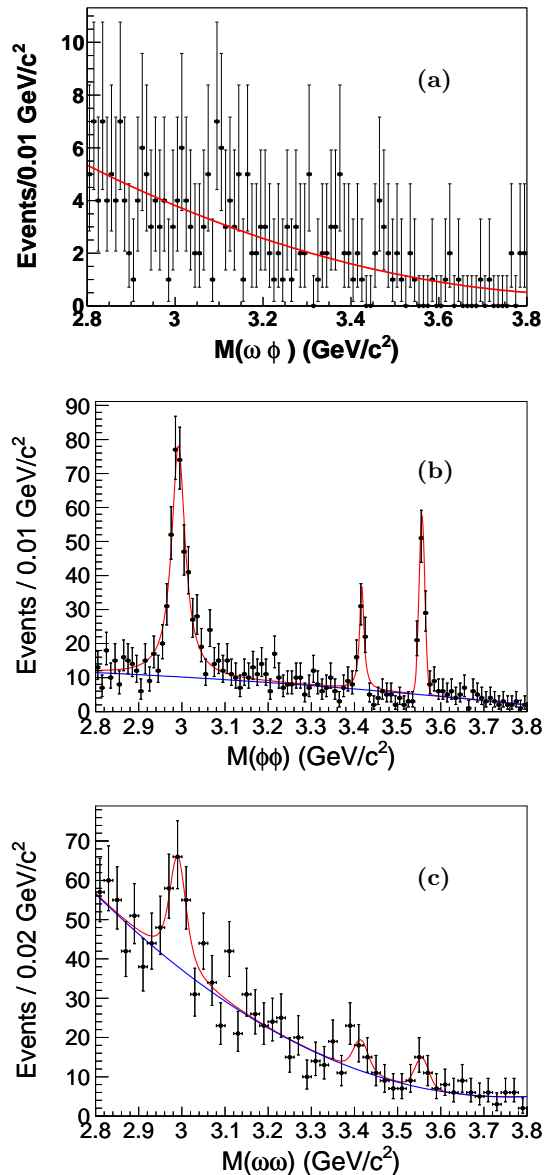


FIG. 3: The invariant mass distributions of (a)  $\omega\phi$ , (b)  $\phi\phi$ , and (c)  $\omega\omega$  combinations in the charmonium mass region with the requirement of  $|\sum \vec{P}_t^*| < 0.1$  GeV/c. The points with error bars are data, and the solid curves are the best fits.

Both the peak position and the peak height predicted in [23] and [24] disagree with our measurements.

We thank the KEKB group for excellent operation of the accelerator; the KEK cryogenics group for efficient solenoid operations; and the KEK computer group, the NII, and PNNL/EMSL for valuable computing and SINET4 network support. We acknowledge support from MEXT, JSPS and Nagoya's TLPRC (Japan); ARC and DIISR (Australia); NSFC (China); MSMT (Czechia); DST (India); INFN (Italy); MEST, NRF, GSDC of KISTI, and WCU (Korea); MNiSW (Poland); MES and RFAAE (Russia); ARRS (Slovenia); SNSF (Switzerland); NSC and MOE (Taiwan); and DOE and NSF (USA).

- [1] See for example the recent review: N. Brambilla *et al.*, *Eur. Phys. J. C* **71**, 1534 (2011).
- [2] S. Uehara *et al.* [Belle Collaboration], *Phys. Rev. Lett.* **104**, 092001 (2010); P. del Amo Sanchez *et al.* [BABAR Collaboration], *Phys. Rev. D* **82**, 011101 (2010).
- [3] C. P. Shen *et al.* [Belle Collaboration], *Phys. Rev. Lett.* **104**, 112004 (2010).
- [4] R. Brandelik *et al.* [TASSO Collaboration], *Phys. Lett. B* **97**, 448 (1980).
- [5] H.-J. Behrend *et al.* [CELLO Collaboration], *Phys. Lett. B* **218**, 493 (1989); H. Albrecht *et al.* [ARGUS Collaboration], *Phys. Lett. B* **217**, 205 (1989); H. Albrecht *et al.* [ARGUS Collaboration], *Phys. Lett. B* **267**, 535 (1991).
- [6] R. L. Jaffe, *Phys. Rev. D* **15**, 267 (1977); R. L. Jaffe, *Phys. Rev. D* **15**, 281 (1977).
- [7] G. Alexander, U. Maor and P. G. Williams, *Phys. Rev. D* **26**, 1198 (1982); G. Alexander, A. Levy and U. Maor, *Z. Phys. C* **30**, 65 (1986).
- [8] Keh-Fei Liu and Bing-An Li, *Phys. Rev. Lett.* **58**, 2288 (1987); N. N. Achasov and G. N. Shestakov, *Phys. Lett. B* **203**, 309 (1988).
- [9] N. N. Achasov and G. N. Shestakov, *Usp. Fiz. Nauk* **161**, 53 (1991) [*Sov. Phys. Usp.* **34**, 471 (1991)].
- [10] H. Albrecht *et al.* [ARGUS Collaboration], *Phys. Lett. B* **332**, 451 (1994).
- [11] H. Albrecht *et al.* [ARGUS Collaboration], *Phys. Lett. B* **374**, 265 (1996).
- [12] A. Abashian *et al.* [Belle Collaboration], *Nucl. Instr. and Methods Phys. Res. Sect. A* **479**, 117 (2002).
- [13] S. Kurokawa and E. Kikutani, *Nucl. Instr. and Meth-*

- ods Phys. Res. Sect. A **499**, 1 (2003), and other papers included in this volume.
- [14] S. Uehara, KEK Report 96-11 (1996). In the generator, the form factor is assumed to be  $1/(1 + Q^2/W^2)$ , where  $Q^2$  is a sign-changed 4-momentum transfer of an electron and represents the virtuality of the photon. [<http://lss.fnal.gov/archive/other1/kek-report-96-11.pdf>].
- [15] C. P. Shen *et al.* [Belle Collaboration], Phys. Rev. D **82**, 051504(R) (2010).
- [16] K. Hanagaki *et al.*, Nucl. Instr. and Methods Phys. Res. Sect. A **485**, 490 (2002).
- [17] Using  $\omega\phi$  as an example,  $z$  is the cosine of the scattering polar angle of  $\phi$  in the  $\gamma\gamma$  C.M. system;  $z^*$  and  $\phi^*$  are the cosine of the helicity angle of  $K^+$  in the  $\phi$  decays and the azimuthal angle defined in the  $\phi$  rest frame with respect to the  $\gamma\gamma \rightarrow \omega\phi$  scattering plane;  $z^{**}$  and  $\phi^{**}$  are the cosine of the helicity angle of normal direction to the decay plane of the  $\omega \rightarrow \pi^+\pi^-\pi^0$  and the azimuthal angle defined in the  $\omega$  rest frame.
- [18] V. L. Chernyak, arXiv:0912.0623.
- [19] H. Nakazawa *et al.* [Belle Collaboration], Phys. Lett. B **615**, 39 (2005); W. T. Chen *et al.* [Belle Collaboration], Phys. Lett. B **651**, 15 (2007); S. Uehara *et al.* [Belle Collaboration], Phys. Rev. D **79**, 052009 (2009); S. Uehara *et al.* [Belle Collaboration], Phys. Rev. D **80**, 032001 (2009); S. Uehara *et al.* [Belle Collaboration], Phys. Rev. D **82**, 114031 (2010).
- [20] S. Uehara *et al.* [Belle Collaboration], Eur. Phys. J. C **53**, 1 (2008).
- [21] K. Nakamura *et al.* (Particle Data Group), Jour. of Phys. G **37**, 075021 (2010).
- [22] Since the  $\eta_c \rightarrow \phi\phi$  signal is significant and the  $\eta_c$  width is relatively large, we also fit with a coherent BW function for the  $\eta_c$ . There are two solutions with equally good fit quality (the goodness of the fit is  $\chi^2/ndf = 0.6$ ). The products of the two-photon decay width and branching fraction  $\Gamma_{\gamma\gamma}\mathcal{B}(\eta_c \rightarrow \phi\phi)$  are  $3.13 \pm 0.55$  eV for the constructive solution, and  $15.7 \pm 1.9$  eV for the destructive solution, where the errors are statistical only.
- [23] G. Alexander, A. Levy and U. Maor, Z. Phys. C **30**, 65 (1986).
- [24] N. N. Achasov, V. A. Karnakov and G. N. Shestakov, Z. Phys. C **36**, 661 (1987).